X-ray photoemission spectroscopy in the Falicov-Kimball model

Nandan Pakhira, A. M. Shvaika, and J. K. Freericks

Phys. Rev. B **99**, 125137 — Published 21 March 2019

DOI: 10.1103/PhysRevB.99.125137

X-Ray Photoemission Spectroscopy in the Falicov-Kimball model

Nandan Pakhira,[1,2] A. M. Shvaika,[3] and J. K. Freericks[4]

[1] *Department of Physics, Indian Institute of Technology, Kharagpur, West Bengal 721302, India.*
[2] *Department of Physics, Kazi Nazrul University, Asansol, West Bengal 713340, India.*
[3] *Institute for Condensed Matter Physics of the National Academy of Sciences of Ukraine, 1 Svientsitskii Street, 79011 Lviv, Ukraine*
[4] *Department of Physics, Georgetown University, Washington, DC 20057, USA.*

We calculate the finite temperature X-ray photo-emission spectroscopy for the Falicov-Kimball model using a Weiner-Hopf sum equation approach. In the metallic state, the core-hole spectral function shows two side peaks corresponding to the creation of a core-hole on an empty site (or a doubly occupied site) and also has two nearly degenerate central peaks (because of our choice of the model parameters) corresponding to the creation of a core-hole on a singly occupied site. The nearly doubly degenerate central peaks merge into a single peak at higher temperatures. In the insulating state, we obtain two peaks and a strongly temperature dependent low-energy peak corresponding to the creation of a core-hole on a thermally excited empty site. These results for the insulating state should be similar to those of the more general Hubbard model. Also, the strong correlations suggest that even without any additional broadening due to Auger like processes, the core-hole lifetime will be short.

I. INTRODUCTION

In a large class of X-ray spectroscopic techniques like X-ray photo-emission spectroscopy (XPS), X-ray absorption spectroscopy (XAS) and resonant inelastic X-ray scattering (RIXS) an incident high energy X-ray photon (typically with an energy $\sim 1-10$ keV) knocks an electron out of a deep core level state either out of the sample (XPS) or to an unoccupied state in the conduction band (XAS and RIXS) thereby creating a hole in the deep core level state. The conduction band electrons then feel a local attractive static potential due to the created core-hole and the system relaxes to a new orthogonal ground state through particle-hole excitations in the conduction band. As a direct consequence of this many body effect, the XAS and XPS show power-law divergences at the threshold energy when $T = 0$. This phenomenon is known as the orthogonality catastrophe, as proposed by Anderson[1]. For noninteracting metals at zero temperature the exponent of the power law and the relative intensity[2–4] of the XPS spectra are well understood. At finite temperature the power-law singularity is cut off by the thermal fluctuations.

Much less is known about the fate of the power law divergence in the XPS spectra of strongly correlated metals and Mott insulators, although this question has been examined by others[5–7]. The theory for strongly correlated XPS can be applied to XPS studies of transition-metal oxide compounds[8–11], which are either Mott insulators or doped Mott insulators with interesting ground state magnetic properties. Cornaglia and Georges[7] have studied core-level photo-emission spectra of the Hubbard model across the metal-insulator transition. The calculated XPS spectra in the metallic phase show an asymmetric power law divergence with an exponent that depends on both the Hubbard interaction U and the core-hole potential Q. With increasing U, the exponent either vanishes continuously (when Q is less than half the bandwidth) or remains nearly constant, but the weight under the peak vanishes (when Q is more than half the bandwidth). This study was limited to zero temperature so it is not able to determine how the behavior changes as the temperature is raised (except to note that an actual power-law divergence only holds exactly at $T = 0$).

Recently, a number of x-ray free-electron lasers have become available which either have, or promise soon to have, revolutionary increases in brightness with narrow pulse widths. Such experimental tools allow one to perform pump/probe experiments with x-rays. The x-rays can act either as a pump or as a probe, and our work here is related to the case where they are employed as a probe. At long delay times, we expect the excited electrons to be approximately described by some form of hot electron model[12]. In this regime, the signatures of an XPS signal will be similar to those of an equilibrium system at high temperature. This is the problem we study here. We find promising evidence that the satellite features of the XPS signal can serve as *in situ* measures of effective temperatures of the electron gas. If so, this probe can have wide applicability for pump/probe experiments that have access to x-ray probes.

We study the temperature dependence of core-hole spectral function in the Falicov-Kimball (FK) model[13], which is also the XPS spectral function because the core-hole level is so far below the Fermi level. The FK-model can be thought of as a special case of the more general Hubbard model in which one of the spin species (say the down spins) is static, while the other spin species (say the up spins) hop through the annealed background of the static spin species with a nearest-neighbor hopping amplitude t. When two electrons of opposite spin are on the same lattice site, they interact with a Coulomb interaction U. Despite its simplicity, the FK-model has a metal-insulator transition for large Coulomb repulsion $U > U_c$ and is exactly solvable via dynamical mean-field theory (DMFT)[14,15]. The local propagator for the itiner-

ant species can be calculated exactly while the propagator for the static species can be calculated systematically by using numerical renormalization group[16–24] (NRG) or the Weiner-Hopf sum equation approach[25–30] (at finite temperature). The most notable difference between the two models is that the metallic state of the FK-model is a non-Fermi liquid[31], while the metallic state in the Hubbard model is a Fermi liquid. The insulating state in both models has the same origin and the charge dynamics in the incompressible Mott insulating state is similar. This relationship between the two models in the insulating phase has been illustrated in studies of non-resonant Raman scattering[32,33].

We note that this work focuses on the Falicov-Kimball model with an extra core-hole. It shares much similarity with the simpler problem of the f-spectral function for the Falicov-Kimball model, where it was recognized early on that x-ray edge physics plays a role[31]. The problem was solved by Brandt and Urbanek[34], whose method was extended and generalized to the Wiener-Hopf approach. The numerical renormalization group was also applied to this problem[20] and shown to be an excellent tool for determining the exponent of the edge singularity in the metallic phase. For high-temperature physics, the Wiener-Hopf approach used here is superior. The organization of the rest of the paper is as follows; In Sec. II, we introduce the core-hole problem, in Sec. III we introduce a mathematical formulation for calculation of the real time Green's function. In Sec. IV, we study the core-hole spectral function using the Wiener-Hopf sum equation approach and finally, in Sec. V, we conclude.

II. CORE-HOLE PROBLEM IN THE FALICOV-KIMBALL MODEL

The Falicov-Kimball[13] was originally proposed as a model for rare-earth compounds near a metal-insulator transition. It involves the interaction between mobile conduction d-electrons and the static localized f-electrons. The model can be applied to real rare earth compounds in an approximate way (in the *incoherent* high temperature region)[35]. The Hamiltonian for the Falicov-Kimball model (in the hole representation, with an additional core hole) is given by

$$\begin{aligned}\mathcal{H} = &-\frac{t^*}{2\sqrt{D}}\sum_{\langle ij\rangle} d_i^\dagger d_j - \sum_i \mu n_{di} + \sum_i (E_f-\mu) n_{fi} \\ &+ \sum_i (E_h-\mu) n_{hi} + \sum_i U n_{di} n_{fi} + \sum_i Q_d n_{di} n_{hi} \\ &+ \sum_i Q_f n_{fi} n_{hi}, \end{aligned} \tag{1}$$

where $t^*/2\sqrt{D}$ is the nearest neighbor hopping amplitude of the itinerant d-holes on a D-dimensional hypercubic lattice and μ is the common chemical potential (we take the limit $D\to\infty$ and use t^* as our energy unit). The

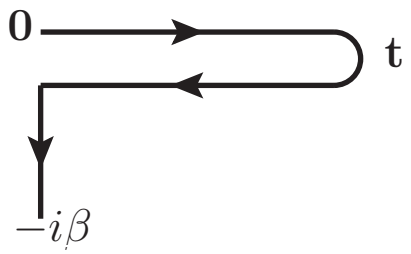

FIG. 1. The Kadanoff-Baym-Keldysh contour. The contour starts at time $t=0$, moves forward in time along the real axis to time t then moves backward in time along the real axis to time $t=0$ and finally moves downwards along the imaginary axis to time $-i\beta$.

symbols $n_{di}=d_i^\dagger d_i$, $n_{fi}=f_i^\dagger f_i$ and $n_{hi}=h_i^\dagger h_i$ are the occupation number operators for the d-hole, f-hole and the core-hole at a given site i, respectively. U is the on-site repulsive Coulomb interaction between the itinerant d-hole and static f-hole, whereas Q_d and Q_f are the repulsive Coulomb interactions between the core-hole and the d-hole and f-hole, respectively. $E_f\sim 1$ eV and $E_h\sim 0.1-10$ keV are the site energies of the f state and the core-hole state, respectively. The case of half-filling ($n_f=n_d=0.5$) corresponds to the choice of $\mu=U/2$ and $E_f=0$; this is the particle-hole symmetric case (in the restricted subspace involving d and f electrons only). Also, under a partial hole-particle transformation $d\to d^\dagger$ and $f\to f^\dagger$, the interaction between the core-hole and the d and f states transforms as $Q_d\to -Q_d$ and $Q_f\to -Q_f$, respectively, *i.e.* becomes attractive instead and the core-hole energy E_h gets shifted to $E_h+Q_d+Q_f$.

Under DMFT, the model reduces to an effective single-impurity problem, described by the following local Hamiltonian

$$\begin{aligned}\mathcal{H}_{\rm loc} = &U n_d n_f + Q_d n_d n_h + Q_f n_f n_h - \mu n_n \\ &+(E_f-\mu) n_f + (E_h-\mu) n_h \end{aligned} \tag{2}$$

along with an effective time-dependent bath (arising from the degrees of freedom at all other sites except the site chosen) to which the d-holes hop in and out. The equilibrium density matrix for the single-impurity problem is given by

$$\rho = \rho_{\rm loc}\mathcal{T}_c \exp\left\{-i\int_c dt' \int_c dt'' d^\dagger(t')\lambda_c(t',t'')d(t'')\right\} \tag{3}$$

where $\rho_{\rm loc}=e^{-\beta H_{\rm loc}}/\mathcal{Z}$, $\mathcal{Z}$ is the partition function (including the effects of the dynamical mean field), $\beta=1/k_BT$ is the inverse temperature and the time-ordering and integration are performed over the Kadanoff-Baym-Keldysh[36,37] contour in Fig. 1. The time dependence of the operators in Eq. (3) are given by the interaction representation with respect to $\mathcal{H}_{\rm loc}$.

The time-translation non-invariant dynamical mean

field $\lambda_c(t,t')$ is given by

$$\lambda_c(t,t') = -\frac{i}{\pi}\int_{-\infty}^{+\infty} d\omega\, \mathrm{Im}\left[\lambda(\omega)\right] e^{i\omega(t'-t)}\left[f(\omega) - \Theta_c(t,t')\right], \tag{4}$$

where $f(\omega) = 1/[1+\exp(\beta\omega)]$ is the Fermi-Dirac distribution function and $\Theta_c(t,t')$ is the Heaviside function on the contour which is equal to 1 when t is ahead of t' on the contour, is equal to 0 when t is behind t' and is equal to $1/2$ when $t = t'$. Note that the dynamical mean field $\lambda(\omega)$ and the chemical potential μ are obtained from the equilibrium solution of the impurity problem without the core-hole. This in effect means that we are treating the creation of the core-hole under the sudden approximation instead of a fully self-consistent non-equilibrium treatment. The creation of the core-hole under the sudden approximation is commonly done because it is consistent with experiments.

Because of the conserved core-hole number, n_h, and the conserved f-hole number, n_f, the full Hilbert space of the core-hole problem can be expressed as the direct sum of the Hilbert spaces in each conserved $\{n_h, n_f\}$ sector. For the spinless case, the total partition function for the single-impurity problem $\mathcal{Z}$ contains four terms $\mathcal{Z}_\alpha \equiv \mathcal{Z}_{n_h n_f}$, each of which corresponds to the partition function for the Hilbert space in the conserved $\{n_h, n_f\}$ sector. We have

$$\mathcal{Z} = \mathcal{Z}_{00} + \mathcal{Z}_{01} + e^{-\beta(E_h-\mu)}\left[\mathcal{Z}_{10} + Z_{11}\right] \tag{5}$$

with

$$\mathcal{Z}_{00} = \left[1+e^{\beta\mu}\right]\prod_m \frac{i\omega_m + \mu - \lambda_m}{i\omega_m + \mu} \tag{6}$$

$$\mathcal{Z}_{01} = e^{\beta(\mu-E_f)}\left[1+e^{\beta(\mu-U)}\right]\prod_m \frac{i\omega_m + \mu - U - \lambda_m}{i\omega_m + \mu - U} \tag{7}$$

$$\mathcal{Z}_{10} = \left[1+e^{\beta(\mu-Q_d)}\right]\prod_m \frac{i\omega_m + \mu - Q_d - \lambda_m}{i\omega_m + \mu - Q_d} \tag{8}$$

$$\mathcal{Z}_{11} = e^{\beta(\mu-E_f-Q_f)}\left[1+e^{\beta(\mu-U-Q_d)}\right] \times \prod_m \frac{i\omega_m + \mu - U - Q_d - \lambda_m}{i\omega_m + \mu - U - Q_d}, \tag{9}$$

where $i\omega_m = i\pi(2m+1)k_BT$ is the fermionic Matsubara frequency and

$$\lambda_m = \int_0^\beta d\tau\, e^{i\omega_m\tau}\lambda(\tau) \tag{10}$$

is the dynamical mean field evaluated at $i\omega_m$. The contour-ordered dynamical mean field λ_c depends on the difference of its two time arguments when both of them lie on the imaginary time axis of the Kadanoff-Baym-Keldysh contour; we also use the notation $\lambda(\tau) = -i\lambda_c(-i\tau, 0)$.

III. REAL TIME GREEN'S FUNCTIONS

We define the contour-ordered Green's function for the core-hole as

$$G_h^c(t,t') = -i\langle \mathcal{T}_c\, h(t)h^\dagger(t')\rangle, \tag{11}$$

where the time ordering is taken along the Kadanoff-Baym-Keldysh contour shown in Fig. 1 and $\langle\cdots\rangle$ corresponds to the trace weighted by the equilibrium density matrix in Eq. (3). We also define the greater Green's function $G^>(t,t') = -i\langle h(t)h^\dagger(t')\rangle$ and lesser Green's function $G^<(t,t') = i\langle h^\dagger(t')h(t)\rangle$, which can all be expressed via

$$G^>(t,t') = -\frac{i}{\mathcal{Z}}\sum_{m,n} e^{-\beta E_m}|\langle m|h|n\rangle|^2 e^{i(E_m-E_n)(t-t')} \tag{12}$$

$$G^<(t,t') = \frac{i}{\mathcal{Z}}\sum_{m,n} e^{-\beta E_n}|\langle n|h^\dagger|m\rangle|^2 e^{i(E_m-E_n)(t-t')} \tag{13}$$

in the eigen basis of the lattice Falicov-Kimball Hamiltonian with the additional core hole in Eq. (1); the eigenstates satisfy $\mathcal{H}|n\rangle = E_n|n\rangle$. Note that we have suppressed the lattice site index in these equations, since the core-hole propagator is independent of the lattice site, but is always local, implying that the two hole creation and destruction operators must be from the same lattice site. Out of these two Green's functions we can construct retarded and advanced Green's functions,

$$G_h^r(t,t') = -i\Theta(t-t')\langle\left[h(t), h^\dagger(t')\right]_+\rangle \tag{14}$$
$$= \Theta(t-t')\left[G_h^>(t,t') - G_h^<(t,t')\right],$$

$$G_h^a(t,t') = i\Theta(t'-t)\langle\left[h(t), h^\dagger(t')\right]_+\rangle \tag{15}$$
$$= \Theta(t'-t)\left[G_h^<(t,t') - G_h^>(t,t')\right], \tag{16}$$

respectively. The symbol $[A,B]_+ = AB + BA$ represents the anti commutator.

Equilibrium problems are time-translation invariant, because there is no preferred time. This is a property shared by the Green's functions, which follows by cyclic invariance of the trace and the fact that the lattice Hamiltonian commutes with itself. Hence, all of the Green's functions discussed here are functions only of $t-t'$. Furthermore, by relating the complex conjugate of a matrix element, to the Hermitian conjugate of the operators in the matrix element, we can also show that

$$\left[G_h^>(t)\right]^* = -G_h^>(-t), \quad \left[G_h^<(t)\right]^* = -G_h^<(-t). \tag{17}$$

The core-hole spectral function $A_h(\omega)$ is then determined from

$$A_h(\omega) = -\frac{1}{\pi}\,\mathrm{Im}\left[G_h^r(\omega + i0^+)\right]. \tag{18}$$

In many cases, one can directly perform an analytic continuation from Matsubara frequencies to real frequencies, but there is no obvious way to do that here[27,28,34].

Instead, one can always formulate the problem on the Kadanoff-Baym-Keldysh contour, and directly determine the Green's function as a function of time. It can then be Fourier transformed to frequency. This is the approach we adopt here. Furthermore, for most core level states involving atomic $1s$ and $2p$ orbitals the core-hole energy is large $E_h \gg 0$ ($E_h \sim 600$ eV). In this limit, the presence of the thermal factor given by $\exp[-\beta(E_h-\mu)]$, completely suppresses the lesser Green's function, which we can approximate by zero. Hence, we have that the greater Green's function is identical to the retarded Green's function in this limit, namely $G_h^r(t) = \Theta(t) G_h^>(t)$. So we only need to compute

$$G_h^>(t) = -i\mathrm{Tr}\Big[\mathcal{T}_c \exp\left\{-i\int_c dt' \int_c dt'' d^\dagger(t')\lambda_c(t',t'')d(t'')\right\} \times h(t)h^\dagger(0)\rho_{\rm loc}\Big], \tag{19}$$

for $t \geq 0$.

We begin by solving the equations of motion for the core-hole operators, given by

$$\frac{dh(t)}{dt} = -i\left[Q_d n_d(t) + Q_f n_f(t) + E_h - \mu\right] h(t), \tag{20}$$

$$\frac{dh^\dagger(\bar{t})}{d\bar{t}} = i\left[Q_d n_d(\bar{t}) + Q_f n_f(\bar{t}) + E_h - \mu\right] h^\dagger(\bar{t}), \tag{21}$$

and substitute their solutions into Eq. (19), yielding

$$G_h^>(t) = -ie^{-i(E_h-\mu)t}\mathrm{Tr}\left[e^{-\beta H_0} e^{-iQ_f n_f t}\, \mathcal{S}_c(t) h(0) h^\dagger(0)\right] \tag{22}$$

where,

$$\mathcal{S}_c(t) = \mathcal{T}_c \exp\left\{-i\int_c dt' \int_c dt'' d^\dagger(t')\lambda_c(t',t'')d(t'') - i\int_c dt' Q_c(t,t') n_d(t')\right\}, \tag{23}$$

with $Q_c(t,t') = Q_d$ for $t' \in [0,t]$ *on the upper branch of the contour only* and zero otherwise. It is due to the lack of time translation invariance of the $Q_c(t,t')$ field that we must use the Kadanoff-Baym-Keldysh formalism for the analytic continuation. Note, however, that the final Green's function will remain time-translation invariant.

Since the core-hole occupation number $n_h = h^\dagger h$ is conserved, we have a projection onto states without a core-hole ($n_h = 0$) only. Furthermore, since n_f is also conserved, we add together the contributions for $n_f = 0$ (top line) and $n_f = 1$ (bottom line). This results in

$$G_h^>(t) = -\frac{i}{\mathcal{Z}} e^{-i(E_h-\mu)t}\mathrm{Tr}\left[e^{\beta\mu n_d}\mathcal{S}_c(t)\right] - \frac{i}{\mathcal{Z}} e^{-i(E_h-\mu)t} e^{-\beta(E_f-\mu)} e^{-iQ_f t}\mathrm{Tr}\left[e^{\beta(\mu-U)n_d}\mathcal{S}_c(t)\right], \tag{24}$$

where the trace is now over the d-holes only.

The evaluation of the remaining traces is straightforward, because the actions are quadratic in the d-electrons. But the steps one needs to follow are a bit involved. Following the methodology employed in the calculation of the f-particle propagator[29], we compute the solution in terms of the functional determinants

$$G_h^>(t) = -ie^{-i(E_h-\mu)t}\left[\frac{\mathcal{Z}_{00}}{\mathcal{Z}}\det{}_{[0,t]}(\mathbb{I} - Q_d G_{00}) + \frac{\mathcal{Z}_{01}}{\mathcal{Z}} e^{-iQ_f t}\det{}_{[0,t]}(\mathbb{I} - Q_d G_{01})\right], \tag{25}$$

where the continuous matrix elements of the Green's functions G_{00} and G_{01} in the determinants are the causal (time-ordered) Green's functions

$$G_{n_h,n_f}(t',t'') = -\frac{i}{\pi}\int_{-\infty}^{+\infty} d\omega e^{-i\omega(t'-t'')}\,\mathrm{Im}\,\mathcal{G}_{n_h,n_f}(\omega) \times \left[f(\omega) - \Theta(t'-t'')\right] \tag{26}$$

defined through the retarded one

$$\mathcal{G}_{n_h,n_f}(\omega) = \frac{1}{\omega + i\delta - \epsilon_{n_h n_f} - \lambda(\omega+i\delta)} \tag{27}$$

with the Fourier transform

$$G_{n_h,n_f}(\omega) = \mathrm{Re}\,\mathcal{G}_{n_h,n_f}(\omega) + i\tanh\frac{\beta\omega}{2}\,\mathrm{Im}\,\mathcal{G}_{n_h,n_f}(\omega). \tag{28}$$

Here the local energies $\epsilon_{n_h n_f}$ are equal $\epsilon_{00} = -\mu$, $\epsilon_{01} = U-\mu$, $\epsilon_{10} = Q_d - \mu$, and $\epsilon_{11} = U + Q_d - \mu$ and the step function $\Theta(t'-t'')$ must be defined as 1 for $t' > t''$ and 0 for $t' \leq t''$ [at equal time values we must have the lesser Green's function with $\Theta(0) = 0$ which produces $in_d(t')$ in Eq. (23), whereas for other frequently used definitions $\Theta(0) = 1$ and $1/2$ we would mistakenly obtain $i(n_d(t')-1)$ and $i(n_d(t')-0.5)$, respectively]. Note that the determinants in Eq. (25) are continuous matrix determinants over finite time intervals ranging from 0 to t and we must recall that the identity matrix is given by a delta function in the time domain.

The continuous time determinants are in the Toeplitz form because the Green's function $G_{n_h,n_f}(t_1,t_2) = G_{n_h,n_f}(t_1-t_2)$ depends only on the difference of the two time arguments. Asymptotic limits ($t \to \infty$) of Toeplitz determinants can be easily calculated by using the Wiener-Hopf sum equation approach and Szegö's theorem[25]. Two of us have also developed systematic finite-time corrections to these asymptotic forms[29,30] and found that the form of the large-time behavior is determined by the winding number of the matrices in Eq. (25), which depends on the analytic properties of the logarithm of the characteristic function

$$C_{n_h,n_f}(\omega) = 1 - Q_d G_{n_h,n_f}(\omega) = 1 - Q_d\,\mathrm{Re}\,\mathcal{G}_{n_h,n_f}(\omega) + iQ_d\tanh\frac{\beta\omega}{2}\,\mathrm{Im}\,\mathcal{G}_{n_h,n_f}(\omega) \tag{29}$$

The imaginary part of this function changes sign at $\omega = 0$ and, depending on the sign of its real part, the logarithm of $C_{n_h,n_f}(\omega)$ is either a monotonic function or possesses

a discontinuity equal to $2\pi i$ at $\omega = 0$. In the first case, where $\mathrm{Re}\, C_{n_h,n_f}(\omega = 0) > 0$, the winding number of the corresponding matrix is equal to zero and the large time asymptotic behavior of the determinant is exponential, giving rise to Lorentzian XPS peak profiles. On the other hand, for the case where $\mathrm{Re}\, C_{n_h,n_f}(\omega = 0) < 0$, the winding number is equal to -1 and the determinants decay to zero much faster at large times producing non-trivial XPS peak profiles.

For the case of the half filled Falicov-Kimball model with a symmetric conduction-electron DOS, we have $\mu = U/2$, $\epsilon_{00} = -U/2$, $\epsilon_{01} = U/2$, and $\mathrm{Re}\,\lambda(0) = 0$, which yields

$$\mathrm{Re}\, C_{00}(0) = 1 - \frac{Q_d\, U/2}{(U/2)^2 + (\mathrm{Im}\,\lambda(0))^2},$$
$$\mathrm{Re}\, C_{01}(0) = 1 + \frac{Q_d\, U/2}{(U/2)^2 + (\mathrm{Im}\,\lambda(0))^2} > 0. \qquad (30)$$

It should be noted that, $\mathrm{Im}\,\lambda(0)$ is connected with the imaginary part of the self-energy via $\mathrm{Im}\,\Sigma(0) = U^2/4\,\mathrm{Im}\,\lambda(0)$, which also determines the lifetime of the single-particle excitations at the chemical potential. One can see that $\mathrm{Re}\, C_{01}(0)$ is always positive which means that the winding number for the second determinant in Eq. (25) is zero and it always decays exponentially for large times. The behavior of the first determinant depends on the Q_d value. For $Q_d < Q_{dc}$, where

$$Q_{dc} = \frac{U}{2} + \frac{2(\mathrm{Im}\,\lambda(0))^2}{U}, \qquad (31)$$

$\mathrm{Re}\, C_{01}(0)$ is also positive and we have exponential decay at large times, whereas for $Q_d > Q_{dc}$, $\mathrm{Re}\, C_{01}(0)$ is negative and the asymptotic behavior of the first determinant is non-exponential; instead it decays much faster at large times. It should be noted, that for the Mott insulator with $\mathrm{Im}\,\lambda(0) = 0$, we have $Q_{dc} = U/2$[38].

While we are not explicitly interested in what happens as $T \to 0$, in this work, one would likely find that the exponential decay in time is modified to a power law decay when the winding number is zero. When this occurs, it will give rise to edge singularities in the spectrum, which are rigorously present only at $T = 0$. The fact that the winding number becomes -1 in the "dirty" metallic phase (with nonzero U), indicates that one can lose edge singularities even in metallic systems if the core-hole interaction strength is large enough.

The finite time Toeplitz determinants can also be calculated through a discretization of the continuous matrix operators and a numerical integration over the Kadanoff-Baym-Keldysh contour. This latter method is found to be accurate in the small time region but becomes numerically intractable in the large time region because of the large matrices involved (due to the use of a fixed step size in time). We adopt a hybrid approach in which we use direct numerical evaluation of the Toeplitz determinants in the small time region and use Szegö's theorem and its finite time corrections to calculate the determinants in the large time region. This approach produces accurate real time Green's functions for all times.

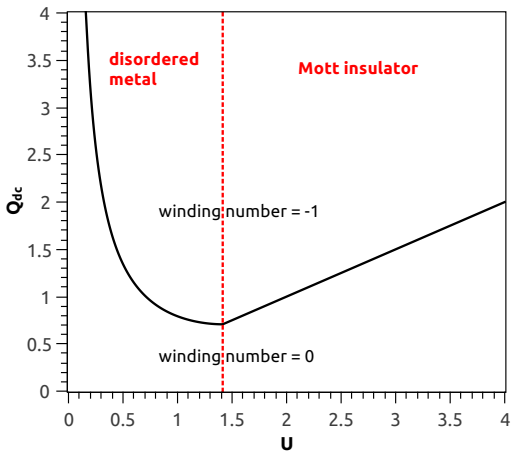

FIG. 2. Critical core-hole potential Q_{dc} for different Coulomb interactions U (black solid line). Note that the Mott phase appears for $U > \sqrt{2}$, as indicated by the dashed line; the core-hole potential chosen in this work is alway larger than U. This implies that we often have winding number of -1.

IV. CORE-HOLE SPECTRAL FUNCTION

We choose the familiar half-filling case which corresponds to $\langle n_d \rangle = \langle n_f \rangle = 0.5$ and $\mu = U/2$ in the absence of the core-hole and as already mentioned we treat the creation of the core-hole under the sudden approximation; *i.e.* the creation of the core-hole does not modify the dynamics of the itinerant d-hole or static f-hole. We also choose hypercubic lattice, which in the limit of large dimensions ($D \to \infty$) has a Gaussian density of states

$$D_0(\epsilon) = \frac{1}{\sqrt{\pi}} \exp\left[-\epsilon^2\right] \qquad (32)$$

where we set $t^* = 1$. In the absence of the core-hole, the Falicov-Kimball model has a Mott insulating ground state for $U > U_c = \sqrt{2}$, when spatial ordering is suppressed. The core-hole spectral function $A_h(\omega)$ is also the XPS response function in the deep core-hole limit. We study the evolution of $A_h(\omega)$ for various temperatures T, interaction strengths U, and core-hole potentials Q_d and Q_f, keeping $Q_d = Q_f$ to reduce the number of parameters.

A. Weakly correlated metal

We first consider the case of a weakly correlated metal with $U = 0.5$. As shown in Fig. 3 (a), the conduction electron spectral function $A_d(\omega)$ has a metallic density of states, with no gap. In Fig. 3 (b) and

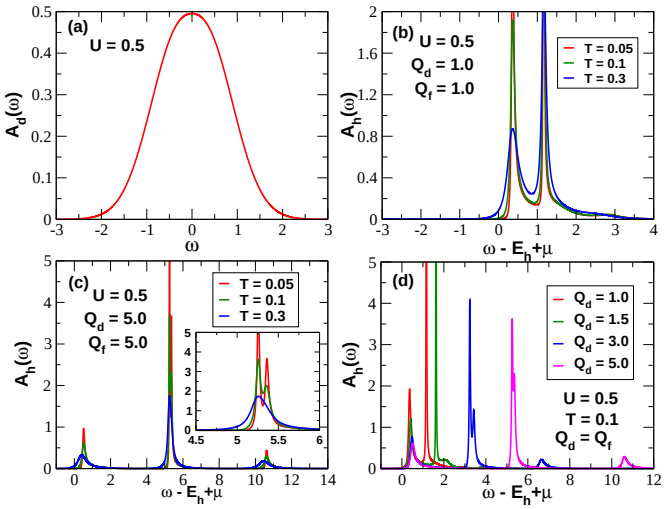

FIG. 3. (Color on-line). Panel (a): Itinerant species spectral function, $A_d(\omega)$. Panel (b) and (c): Temperature dependence of the core-hole spectral function, $A_h(\omega)$, for small ($Q_d = Q_f = 1.0$) and large ($Q_d = Q_f = 5.0$) core-hole potentials. Inset Panel (c): Blown up region near the central peak. Axis labels are the same as in the main panel. Panel (d): Evolution of $A_h(\omega)$ for various core-hole potentials $Q_d = Q_f$ for a given temperature $T = 0.1$. Parameters used for the calculations are all indicated in the figures.

(c), we show the temperature evolution of the core-hole spectral function for small $Q_d = Q_f = 1.0$ and large $Q_d = Q_f = 5.0$ core-hole potentials. The term small and large is with respect to U. $A_h(\omega)$ in Fig. 3(b) shows two distinct peaks and a very broad hump whereas in Fig. 3(c) we clearly see three distinct peaks. The peak structure can be easily understood from the atomic limit picture. Using the equation of motion, we can calculate the retarded core-hole Green's function as $\hat{G}^r_h(\omega) = (\omega + i\eta - E_h + \mu - Q_d\hat{n}_d - Q_f\hat{n}_f)^{-1}$, where one needs to insert the localized hole fillings for each sector. So, if we plot $A_h(\omega)$ as a function of $\omega - E_h + \mu$ then we will see two delta function peaks at 0 and Q_d for $n_f = 0$ and two delta function peaks at Q_f and $Q_d + Q_f$ for $n_f = 1$. Because of the choice $Q_d = Q_f$ through out the calculation the two peak positions at Q_d and Q_f are degenerate. Note that the distance between two peaks in each of the conserved n_f sectors is Q_d. Now once we couple the local Hamiltonian to the dynamical mean field, then each of the delta function peaks gets broadened due to finite lifetime of the atomic levels. Also, their peak position is shifted too. Most interestingly, the distance between the two peaks in each of the conserved n_f sectors still remains equal to $\sim Q_d$. This is due to the fact that the core-hole–d-hole interaction shifts each of the d-hole levels by the same amount, namely $\sim Q_d$.

In Fig. 3(b), the peak near $\Omega \equiv \omega - E_h + \mu = 0$ corresponds to the core-hole being created on a site not occupied by either a d- or f-hole. Whereas the peak at $\Omega \simeq 1.0$ corresponds to a nearly degenerate double peak, where the core-hole is created on a site either occupied by a d or f hole. The broad shoulder at $\Omega \simeq 2.0$ corresponds to the case where the core-hole is created on a site doubly occupied by both a d and f-hole. With increasing core-hole potentials $Q_d = Q_f$, the doubly degenerate central peak gets split as shown in the inset of Fig. 3(c). This is due to the fact that local d-holes directly hybridize with the bath which shifts its energy and width, whereas the f-hole only indirectly sees the fluctuating bath through its interaction with the local d-hole; therefore, it has different self-energy effects when compared to the d-hole. Thermal broadening again smears the two peaks and we obtain one broad central peak at high temperature ($T = 0.3$).

The integrated spectral weight under the central peak is much larger than that of the other two peaks. This corresponds to the fact that at half filling the excited core-hole would more probably be created at singly occupied sites rather than at unoccupied or doubly occupied sites. With increasing temperature the integrated weight under the two side peaks increases and that under the central peak decreases. This is because thermally excited sites create a pair of empty and doubly occupied sites at the expense of two singly occupied sites so the probability that the excited core-hole will be created at one of those sites increases with temperature.

In Fig. 3(d), we show the systematic evolution of $A_h(\omega)$ at a fixed temperature $T = 0.1$ for various core-hole potentials. The main feature is that the peaks corresponding to the excitation of the core-hole onto singly or doubly occupied sites shifts farther and farther from the edge peak. It also appears that peaks are losing intensity, but since the integrated spectral weight is always equal to one, this is just an illusion—the change in peak heights is compensated by a change in their width.

One may ask, where is the edge singularity? In spite of the fact that for $U = 0.5$ we are in the metallic phase, the shape of the peaks is different depending on the Q_d value and whether we are above or below the curve in Fig. 2. For $Q_d = 1$, we are below the curve, $Q_d < Q_{dc}$, and for both contributions in Eq. (25) we observe sharp edge singularity peaks. As the temperature is lowered, one of the peaks becomes very sharp with a high amplitude and eventually it gives rise to a divergent signal with the power-law divergence occurring at $T = 0$[30]. For the larger Q_d values in Fig. 3(d), we are above the curve in Fig. 2, $Q_d > Q_{dc}$, and the low-energy edge peak becomes smooth without displaying any singularity features, whereas the high energy one still does. It is a joint effect of the Coulomb interaction U and the core-hole potential Q_d, which suppresses the edge singularity. This feature is not noticed in previous publications on the edge singularity either because it does not occur for a pure metallic case with $U = 0$[2–4] or because of an approximate treatment of the electron correlations, which misses this effect. We can see that the edge singularity clearly disappears at nonzero temperature. Our focus

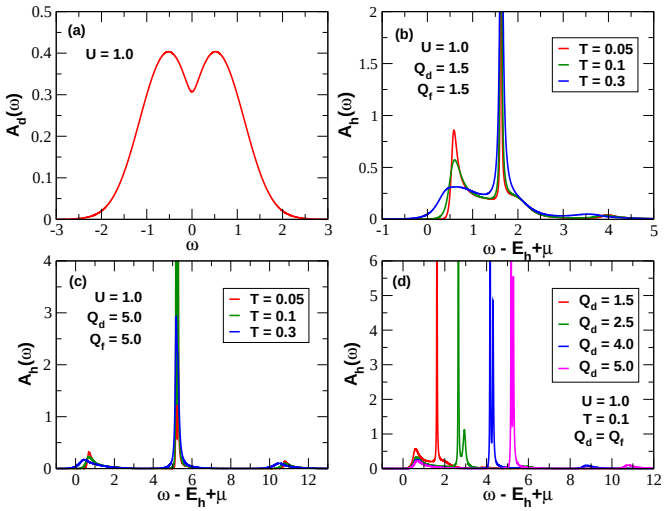

FIG. 4. (Color on-line) Panel (a) Conduction-electron spectral function with its pseudo-gap structure. Panel (b) and (c) Temperature dependence of the core-hole spectral function for moderate ($Q_d = Q_f = 1.5$) and large ($Q_d = Q_f = 5.0$) core-hole potentials. Panel (d) : Evolution of the core-hole spectral function for various core-hole potentials $Q_d = Q_f$ at a fixed temperature $T = 0.1$. The parameters used for the calculations are all indicated in the figures.

here is on how this behavior changes at higher temperatures, and we can see that the behavior dramatically changes.

B. Strongly correlated metal

Next, we consider the case of a strongly correlated metal. We choose $U = 1.0$. The conduction-electron density of states $A_d(\omega)$, is shown in Fig. 4(a), and illustrates a pseudo-gap forming near the chemical potential. Figure 4 panel (b) and (c), plot the temperature evolution of the core-hole spectral function for moderately ($Q_d = Q_f = 1.5$) and large ($Q_d = Q_f = 5.0$) core-hole potentials, respectively. In both cases we have $Q_d > Q_{dc}$ and one of the main features we see is that the central peak, which originates from the second term in Eq. (25) with zero winding number, is narrowing and concentrating more spectral weight, as the weight on the empty and doubly occupied sites goes down. As we increase the core-hole potentials to large values the intensity of the low energy edge peak decreases whereas the central one increases while its width decreases. This is due to increased self-energy effects arising when we put a core-hole onto a site already occupied by a d or f-hole. The side peaks are well separated from the central peak and their intensity and integrated spectral weight under these peaks are reduced compared to the weakly correlated case.

C. Small-gap Mott insulator

As we increase U above $U_c = \sqrt{2}$ we get into the Mott insulating phase. We choose $U = 2.0$ which gives an insulator with a small gap, $\Delta_{\rm gap} \simeq 0.25$. In panel (a) of Fig. 5, we show the spectral function of the d-hole which clearly shows two Hubbard bands centered around $\pm\frac{U}{2}$ and separated by the insulating gap, $\Delta_{\rm gap}$. Of course, it is well known that for the $D = \infty$ hyper cubic lattice the Mott insulating density of states never has a true "gap" as there are always exponentially small density of states inside the "gap region."

Figure 5 panels, (b) and (c), show the core-hole spectral function $A_h(\omega)$ for moderately large $Q_d = Q_f = 2.5$ and large $Q_d = Q_f = 5.0$ core-hole potentials. In the insulating state at zero temperature, a core-hole can only be created on a site which is occupied by either a d-hole or an f-hole. This gives rise to single peak in each of the two conserved sectors of $n_f = 0$ and $n_f = 1$. For $Q_d = Q_f = 2.5$ we see a very sharp near δ-function peak at $\Omega \sim Q_f$ on top of very broad asymmetrical spectral feature. The sharp peak corresponds to the creation of a core-hole on a site already occupied by an f-hole. The sharpness of the peak arises due to both the static nature of the f-hole and the lack of core-hole screening effects in the insulating state thereby making the core-hole state very long lived. The broad asymmetrical part of $A_h(\omega)$ corresponds to the creation of a core-hole on a site occupied by a d-hole. This part consists of a broad peak near $\Omega \sim Q_d$ on top of a broad background. As already mentioned, due to lack of screening effects in the insulating states and strong self-energy effects of the d-hole, the core-hole state is short lived. The width of the broad spectral feature is nearly equal to the width of the lower Hubbard band. At finite temperature, some of the sites become unoccupied while others becomes doubly occupied and creation of core-hole on either of these two sites gives rise to additional side band peaks. The low energy part of the XPS spectra corresponding to the creation of a core-hole on an empty site, which originates from the first term in Eq. (25) with nonzero winding number ($Q_d > Q_{dc}$), does not display any edge singularity. Instead, it mimics the d-electron DOS with lower and upper Hubbard bands separated by the Mott gap of the size $\Delta_{\rm gap}$, which is now temperature dependent. The peak corresponding to the creation of a core-hole on the doubly occupied site is extremely weak (nearly invisible on the scale of the plot) and has negligible spectral weight under it.

With increasing core-hole potentials, the peak at $\Omega \sim Q_f$ corresponding to core-hole excitation into the $n_f = 1$ manifold largely remains the same and only shifts to higher energies, but the spectral features at the low energy XPS edge corresponding to a core-hole excitation onto the $n_f = 0$ manifold shows qualitative changes as plotted in panels (c) and (d). With increasing Q_d, the broad peak from the upper Hubbard band is enhanced in its high energy part with the further creation of a

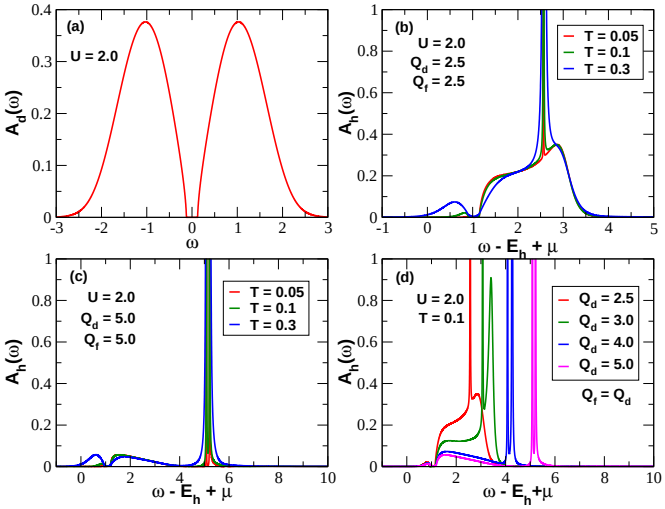

FIG. 5. (Color on-line) Panel (a) Conduction-electron spectral function, $A_d(\omega)$ in the Mott insulator phase. Panels (b) and (c) Core-hole spectral function, $A_h(\omega)$, for moderately large ($Q_d = Q_f = 2.5$) and large ($Q_d = Q_f = 5.0$) core-hole potentials. The peak corresponding to a core-hole excitation onto the doubly occupied manifold has a small spectral weight. Panel (d) Evolution of $A_h(\omega)$ for various core-hole potentials $Q_d = Q_f$ at fixed temperature $T = 0.1$.

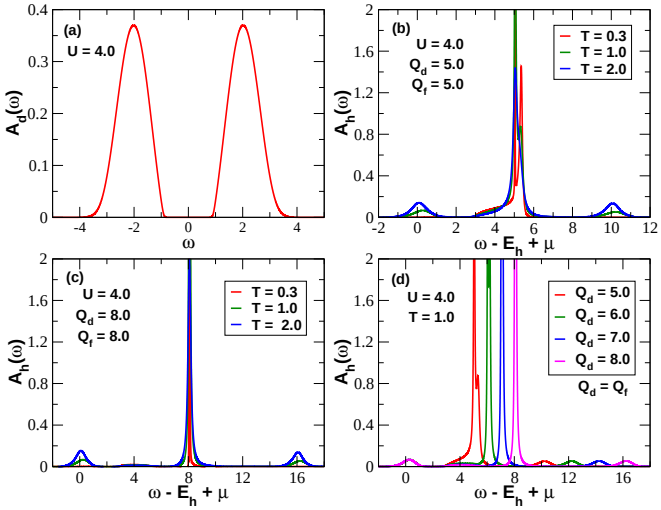

FIG. 6. (Color on-line) Panel (a) The d-hole spectral function $A_d(\omega)$ in a strong Mott insulator. Panel (b) and (c) Core-hole spectral function, $A_h(\omega)$, for large ($Q_d = Q_f = 5.0$) and very large ($Q_d = Q_f = 8.0$) core-hole potentials, respectively. For temperatures larger than 1, side peaks corresponding to core-hole excitations into empty and doubly occupied manifold are clearly visible. Panel (d) Evolution of $A_h(\omega)$ with core-hole potentials $Q_d = Q_f$ for fixed temperature $T = 1.0$.

narrow peak at $\Omega \sim Q_d$ which gets gradually pushed out to higher energy and gradually separates out of the broad background. Also, the core-hole lifetime increases, as is evident from the narrowing and diverging peak at $\Omega \sim Q_d$. This is mainly due to the fact that the excited core-hole goes into the upper Hubbard band and its decay rate decreases with increasing Q_d as the d-hole density of states involved in the decay process decreases with increasing Q_d. Due to the same reason, the integrated spectral weight under the broad background also decreases, while its width remains nearly same.

D. Large gap Mott insulator

Finally we choose $U = 4.0$ to simulate a strong Mott insulator. In panel (a) of Fig. 6, we show the spectral function for the d-hole which clearly shows two Hubbard bands separated by a large insulating gap, $\Delta_{\rm gap} \simeq 1.8$. In this case, the size of the insulating gap is much larger than the hopping. In Fig. 6 panels (b) and (c), we show the core-hole spectral function $A_h(\omega)$ for two core-hole potentials $Q_d = Q_f = 5.0$ and $Q_d = Q_f = 8.0$, respectively. Because of the presence of a large insulating gap in d-hole spectral function and strong correlation effects, the core-hole spectral functions shows negligible temperature dependence for $T \ll 1$. Therefore, we choose temperatures equal to or larger than 1. At the low temperature of $T = 0.3$, we see the two familiar spectral features corresponding to the core-hole being excited to two singly occupied manifolds. The peak at $\Omega \sim Q_d$ is much sharper and the broad spectral features have much less intensity compared to the case of small gap Mott insulator. This is mainly due to reduced density of states and increased correlation effects. For larger $Q_d = Q_f = 8.0$, the broad spectral features have vanishingly small spectral intensity at $T = 0.3$ as shown in panel (c).

As we increase temperature equal to or larger than the hopping, the two nearly degenerate sharp peaks broaden and eventually merge into a single broad peak. Also, there is clear development of two additional spectral peaks at $\Omega \sim 0$ and $\Omega \sim Q_d + Q_f$, which corresponds again to the creation of the core-hole on a thermally excited empty or doubly occupied site, and the peak from the lower Hubbard band at $\Omega \sim 0$ becomes larger than the one from the upper Hubbard band at $\Omega \sim U$.

In panel (d), we show the evolution of $A_h(\omega)$ with various core-hole potentials $Q_d = Q_f$ for $T = 1.0$. With increasing core-hole potentials the peaks at $\Omega \sim Q_d, Q_f$ becomes narrower and gradually merge into a well defined Lorentzian peak which separates out of the broad background. Other peaks at the $\Omega \sim 0$ edge, which comes from the lower Hubbard band, and at $\Omega \sim Q_d + Q_f$, do not change their shape with the increase of the core-hole potentials and are observed only at high enough temperatures.

V. CONCLUSIONS

In conclusion, we have calculated the finite temperature core-hole propagator (XPS spectrum) in the Falicov-Kimball model using the Weiner-Hopf sum equation approach. We have studied the core-hole spectral function, $A_h(\omega)$ for various interaction strengths U and core-hole potentials $Q_d = Q_f$.

While the features of the weakly correlated metal and for for small core-hole potential, $Q_d < Q_{dc}$ are what we would expect at nonzero temperature—they have the power-law singularity suppressed and the spectral features broadened, as we enter the Mott phase and/or increase the core-hole potential, $Q_d > Q_{dc}$, and the system continuously evolves into a different type of spectral function. Whereas, the features of the Mott phase are predictible because the Mott insulator strongly suppresses doubly occupied and empty sites, hence the peaks associated with hole creation on those sites is sharply reduced, the suppression of one of the edge singularities for large core-hole potential $Q_d > Q_{dc}$ is something new and less understood and we explain it by the joint effect of the on-site Coulomb interaction U and the core-hole potential Q_d. In the Mott phase and at finite temperatures, we observe sharp peaks which can be attributed to edge singularities, but we also do not see any clear indication that there is a power-law singularity at $T = 0$ anymore but rather a δ-peak (but we did not study this point in detail).

If we use these results to try to predict what the behavior of time-resolved XPS spectra would look like, we need to be aware of a few issues. First, we would expect the generic broadening of features and enhancement of the satellite peaks as the system absorbs more energy from the light pulse. Second, we also anticipate significant broadening of the sharp peaks in the spectra due to the probe pulse widths. Nevertheless, there are a number of interesting results one can predict could be extracted from such data. This includes the interaction energies U, Q_d, and Q_f, which can be extracted by examining the separations of different peaks. Since the spectral line shapes change so much with temperature, they might be able to be used as effective thermometers for the hot electron gases. Finally, an analysis of the weights in the satellite bands will yield information about the densities of empty and doubly occupied sites, which may be one of the more direct ways to measure doublon occupancy in the system.

What implications does this work have for more general models like the Hubbard model? The metallic phases are difficult to compare when we are below the coherence temperature of the Hubbard model, because the Falicov-Kimball model is not a Fermi liquid. But at higher temperatures, or in the insulating phase, we expect the behavior to be more similar. We already know from Raman scattering studies that the charge dynamics in the insulators are similar[32,33]. The nearly delta function peak corresponding to the creation of a core-hole on a site occupied by a static f-hole will certainly be absent in the case of Hubbard model (instead it will be broadened like the d-hole contribution). So, we do expect that the temperature-dependent broad asymmetrical peak together with the small low energy peak corresponding to creation of a core-hole on a thermally excited empty site will survive in the Hubbard model. Also, the broad nature of this peak suggests that even without any additional broadening due to Auger-like non-radiative processes, the core-hole lifetime will be short.

ACKNOWLEDGEMENTS

The work at Georgetown was supported by the Department of Energy, Office of Basic Energy Sciences, Division of Materials Sciences and Engineering (DMSE) under contract No. DE-FG02-08ER46542 (JKF and NP). NP also acknowledges financial support from IIT, Kharagpur where part of the manuscript was written. JKF also acknowledges support from the McDevitt Bequest at Georgetown. Fig. 1 in this paper is created using open source software JAXODRAW and the original reference has been duly cited in Ref.[39].

[1] P. W. Anderson, Phys. Rev. Lett. **18**, 1049 (1967).
[2] G. D. Mahan, Phys. Rev. **163**, 612 (1967).
[3] P. Nozières and C. T. De Dominicis, Phys. Rev. **178**, 1097 (1969).
[4] S. Doniach and M. Sunjić, J. Phys. C **3**, 285 (1970).
[5] D. K. K. Lee and Y. Chen, Phys. Rev. Lett. **69**, 1399 (1992).
[6] V. Meden, P. Schmitteckert, and N. Shannon, Phys. Rev. B **57**, 8878 (1998).
[7] P. S. Cornaglia and A. Georges, Phys. Rev. B **75**, 115112 (2007).
[8] K. Horiba, M. Taguchi, A. Chainani, Y. Takata, E. Ikenaga, D. Miwa, Y. Nishino, K. Tamasaku, M. Awaji, A. Takeuchi, M. Yabashi, H. Namatame, M. Taniguchi, H. Kumigashira, M. Oshima, M .Lippmaa, M. Kawasaki, H. Koinuma, K. Kobayashi, T. Ishikawa, and S. Shin, Phys. Rev. Lett. **93**, 236401 (2004).
[9] H.-D. Kim, H.-J. Noh, K. H. Kim, and S.-J. Oh, Phys. Rev. Lett. **93**, 126404 (2004).
[10] M. Taguchi, A. Chainani, N. Kamakura, K. Horiba, Y. Takata, M. Yabashi, K. Tamasaku, Y. Nishino, D. Miwa, T. Ishikawa, S. Shin, E. Ikenaga, T. Yokoya, K. Kobayashi, T. Mochiku, K. Hirata, and K. Motoya, Phys. Rev. B **71**, 155102 (2005).
[11] G. Panaccione, M. Altarelli, A. Fondacaro, A. Georges, S. Huotari, P. Lacovig, A. Lichtenstein, P. Metcalf, G.

Monaco, F. Offi, L. Paolasini, A. Poteryaev, M. Sacchi, and O. Tjernberg, Phys. Rev. Lett. **97**, 116401 (2006).
[12] P. B. Allen, Phys. Rev. Lett. **59**, 1460 (1987).
[13] L. M. Falicov and J. C. Kimball, Phys. Rev. Lett. **22**, 997 (1969).
[14] U. Brandt, and C. Mielsch, Z. Phys. B : Condens. Matter **75**,365(1989).
[15] J. K. Freericks and V. Zlatić, Rev. Mod. Phys. **75**, 1333 (2003).
[16] K. G. Wilson, Rev. Mod. Phys. **47**, 773 (1975).
[17] H. R. Krishna-murthy, J. W. Wilkins, and K. G. Wilson, Phys. Rev. B **21**, 1003 (1980).
[18] H. R. Krishna-murthy, J. W. Wilkins, and K. G. Wilson, Phys. Rev. B **21**, 1044 (1980).
[19] R. Bulla, T. A. Costi, and Th. Pruschke, Rev. Mod. Phys. **80**, 395 (2008).
[20] F. B. Anders, and G. Czycholl, Phys. Rev. B **71**, 125101 (2005).
[21] F. B. Anders and A. Schiller, Phys. Rev. Lett. **95**, 196801 (2005).
[22] F. B. Anders and A. Schiller, Phys. Rev. B **74**, 245113 (2006).
[23] R. Peters, T. Pruschke, and F. B. Anders, Phys. Rev. B **74**, 245114 (2006).
[24] A. Weichselbaum and J. von Delft, Phys. Rev. Lett. **99**, 076402 (2007).
[25] B. M. McCoy and T. T. Wu, *The two dimensional Ising model*, Harvard University Press, Cambridge, MA, 1973.
[26] V. Janis, Int. J. Mod. Phys. B,**11**, 3433 (1997).
[27] V. Zlatić, J. K. Freericks, R. Lemański, and G. Czycholl, Phillos. Mag. B **81**, 1443 (2001).
[28] J. K. Freericks, V. M. Turkowski, and V. Zlatić, Phys. Rev. B **71**, 115111 (2005).
[29] A. M. Shvaika and J. K. Freericks, Condens. Matter Phys. **11**, 425 (2008).
[30] A. M. Shvaika and J. K. Freericks, Condens. Matter Phys. **15**, 43701 (2012).
[31] Q. Si, G. Kotliar, and A. Georges, Phys. Rev. B **46**, 1261(R) (1992).
[32] J. K. Freericks and T. P. Devereaux, Phys. Rev. B **64**, 125110 (2001).
[33] J. K. Freericks, T. P. Devereaux, and R. Bulla, Phys. Rev. B **64**, 233114 (2001).
[34] U. Brandt and M. P. Urbanek, Z. Phys. B: Condens. Matter **89**, 297 (1992).
[35] V. Zlatić and J. K. Freericks, Acta Phys. Pol. B **32**, 3253 (2001).
[36] L. P. Kadanoff and G. Baym, *Quantum statistical mechanics*, Benjamin, New York, 1962.
[37] L. V. Keldysh, Zh. Eksp. Teor. Fiz. **47**, 1945 (1964) [Sov. Phys. JETP **20**, 1018 (1965)].
[38] A similar analysis of the f-particle propagator gives an equation for the critical U: $U/2 = -\mathrm{Im}\,\lambda(0)$ with solution $U_0 = 0.8655$ for the Gaussian DOS[29], whereas for the Bethe lattice with a semicircular DOS, we have $U_0 = W/\sqrt{2}$ and $Q_{dc} = W^2/2U$ for the metallic phase with $U < W$ and $Q_{dc} = U/2$ for the Mott insulator with $U > W$.
[39] D. Binosi and L. Theußl, Comput. Phys. Commun. **161**, 76 (2004).